ADVANCED FUNCTIONAL MATERIALS
www.afm-journal.de

Multiphoton Absorption Stimulated Metal Chalcogenide Quantum Dot Solar Cells under Ambient and Concentrated Irradiance

Bo Hou, Byung-Sung Kim, Harrison Ka Hin Lee, Yuljae Cho, Paul Giraud, Mengxia Liu, Jingchao Zhang, Matthew L. Davies, James R. Durrant, Wing Chung Tsoi, Zhe Li, Stoichko D. Dimitrov, Jung Inn Sohn,* SeungNam Cha,* and Jong Min Kim*

Colloidal metal chalcogenide quantum dots (QDs) have excellent quantum efficiency in light–matter interactions and good device stability. However, QDs have been brought to the forefront as viable building blocks in bottom-up assembling semiconductor devices, the development of QD solar cell (QDSC) is still confronting considerable challenges compared to other QD technologies due to their low performance under natural sunlight, as a consequence of untapped potential from their quantized density-of-state and inorganic natures. This report is designed to address this long-standing challenge by accessing the feasibility of using QDSC for indoor and concentration PV (CPV) applications. This work finds that above bandgap photon energy irradiation of QD solids can generate high densities of excitons via multi-photon absorption (MPA), and these excitons are not limited to diffuse by Auger recombination up to 1.5×10^{19} cm^{-3} densities. Based on these findings, a 19.5% (2000 lux indoor light) and an 11.6% efficiency (1.5 Suns) have been facilely realized from ordinary QDSCs (9.55% under 1 Sun). To further illustrate the potential of the MPA in QDSCs, 21.29% efficiency polymer lens CPVs (4.08 Suns) and viable sensor networks powered by indoor QDSCs matrix have been demonstrated.

1. Introduction

Energy is important for the evolution of humans, and human civilization has eternally searched for sustainable energy supply.[1] A milestone invention, the solar cell, allows abundant solar energy to be directly converted into electricity with low carbon emissions and geographical limitations.[1–3] III–V multi-junction cells and "flat-plate" silicon technologies are the primary workhorse for photovoltaics (PVs) under varied irradiation conditions, including flat panel solar cells, concentration PVs (CPVs), outer space solar panels, and indoor solar cells, which deliver considerable power to our daily life. However, several confronting challenges need to be addressed, such as higher cost and lower sustainability and flexibility.[2a,4,5] Compared to most photoactive materials in the emerging 3rd generation PV, colloidal

B. Hou
Department of Physics and Astronomy
Cardiff University
Cardiff CF24 3AA, UK

B.-S. Kim, P. Giraud
Department of Engineering Science
University of Oxford
Oxford OX1 3PJ, UK

H. K. H. Lee, M. L. Davies, J. R. Durrant, W. C. Tsoi
SPECIFIC
College of Engineering
Swansea University
Swansea SA1 8EN, UK

The ORCID identification number(s) for the author(s) of this article can be found under https://doi.org/10.1002/adfm.202004563.

[+]Present address: Cavendish Laboratory, University of Cambridge, J. J. Thomson Avenue, Cambridge CB3 0HE, UK

DOI: 10.1002/adfm.202004563

Y. Cho
University of Michigan-Shanghai Jiao Tong University Joint Institute
Shanghai Jiao Tong University
800 Dong Chuan Road, Minhang District, Shanghai 200240, China

M. Liu[+]
Department of Electrical and Computer Engineering
University of Toronto
10 King's College Road, Toronto, Ontario M5S 3G4, Canada

J. Zhang
Department of Biostatistics and Bioinformatics
Emory University
Atlanta, GA 30322, USA

J. R. Durrant
Department of Chemistry
Imperial College London
London SW7 2AZ, UK

Z. Li
School of Engineering and Materials Science (SEMS)
Queen Mary University of London
London E1 4NS, UK

metal chalcogenide quantum dot solar cells (QDSCs) are a unique class of PVs that suffer no compromise between high theoretical efficiency, stability, and low-cost.[6] However, due to their low performance under simulated sunlight, the development of QDSC is lagging behind other QD technologies such as light-emitting diodes[7] and photodetectors.[8]

Lead sulfide (PbS) QDSCs have an excellent ambient tolerance, the broad spectrum for high solar harvesting efficiency, atomic-like energy-level quantization, and rough surface nature, which have demonstrated tremendous promise in solar cells (≈13% power conversion efficiency [PCE]),[9–14] as well as the rapid developed infrared PVs.[11,15] The atomic like quantization that is the presence of discrete energy levels at the valence and conduction bands and the relatively easy way of manipulating the energy of these levels make QDs distinctly different materials from all other semiconductors.[16–18] In particular, above bandgap light excitation of the QDs can thus lead to multiexciton generation (MEG) and multi-photon absorption (MPA),[19] where the latter opens opportunities for developing PV technology operating at broad light intensity ranges from very low for indoor applications to very high for concentrated solar technologies.[20,21] Therefore, focusing on MPA, QDs are fascinating objects for the exploration of new photoconversion avenues since they can offer unique properties or combinations of features, such as active photon-absorption layers.[5,10,13,16,18,22]

Herein, we report that PbS QDSCs can efficiently convert photon energies into electricity under a very broad range of light conditions mediated by the MPA process. Ultrafast transient absorption spectroscopy (TAS) analysis of the response of PbS QD solid films to various excitation conditions reveal that the strongly coupled QD in the device stack generate a very high density of relatively mobile excitons with interdot hopping times in the range of tens of picoseconds which are also not limited by Auger recombination processes up to 1.5×10^{19} cm^{-3} exciton densities. In order to demonstrate this capability in functioning devices, we evaluated the performance of QDSCs under indoor and concentrated solar irradiation of over four decades of intensities (0.01 to 1000 mW cm^{-2}) and observed that the devices exhibit a continuous linear increase in short-circuit current density (J_{sc}) and a semi-logarithmic increase in open-circuit voltage (V_{oc}). In addition, we fabricated a polymer lens integrated QD concentration CPV and achieved high PCE 21.29% as well as hundreds of hours of a high irradiance operational stability. For the practical perspective of the QDSCs, we demonstrate that QDSCs can successfully power multiple indoor sensor platforms and have a considerable high-energy conversion performance under simulated, real-world sun insolation. Our work demonstrates that QDs should be considered as a serious option for indoor PVs and low concentration CPVs and highlights areas for a further focus of research activities.

S. D. Dimitrov
School of Biological and Chemical Sciences
Queen Mary University of London
London E1 4NS, UK
E-mail: s.dimitrov@qmul.ac.uk
J. I. Sohn
Division of Physics and Semiconductor Science
Dongguk University
Seoul 100-715, Republic of Korea
E-mail: junginn.sohn@dongguk.edu
S. Cha
Department of Physics
Sungkyunkwan University
Suwon 16419, Republic of Korea
E-mail: chasn@skku.edu
J. M. Kim
Department of Engineering
University of Cambridge
Cambridge CB3 0FA, UK

2. Results and Discussion

This study is focused on PbS-based QDSCs and their light–matter interactions under various irradiance with a first excitonic peak at approximately 1000 nm (Bandgap energy ≈1.24 eV). The conventional two-step "synthesis to ligand-exchange" processed ordinary QDSCs (with one Sun PCE of ≈9%) were chosen as testbeds, where the device stack QD solid films were formed through soaking ligands (e.g., tetrabutylammonium iodide, TBAI) on a spinning QD film.[9,23,24] As shown in the **Figure 1**a, the optimal ratio of the photo-generated charge carriers by the QDSC to the number of incident photons at a given wavelength (EQE and IQE spectra) well match the spectral window from indoor and solar irradiance, which suggests a rational utilization of the large population of short wavelength photons (e.g., 350 to 800 nm) in concentrated or high intensity indoor light can be beneficial for high-performance PV devices.[3,6,18,25] The electron microscopy images (Figure S1, Supporting Information) and absorption spectra (Figure S2, Supporting Information) of the as-prepared PbS QDs confirm the typical excitonic characteristics of interband optical transitions in a monodispersed, dimensionally confined system.[26]

We used ultrafast TAS, a pump-probe optical spectroscopy method sensitive to photogenerated excitons and charges, to investigate the response of QDSCs under different light conditions (Figure 1b). TAS measurements were carried out with solution and thin film samples of PbS QD with an oleic acid (QD-OA) ligand. Shown in Figure S2, Supporting Information, the typical transient absorption spectrum of the samples is dominated by the bleach of the $1S_h$-$1S_e$ absorption. Figure 1C presents the intensity-dependent kinetics of the bleach maximum of the film QD-OA and Figure S3, Supporting Information, presents the excitation wavelength dependent bleach kinetics of the solution QD-OA, which reveal the characteristic for these type of particles' picosecond Auger recombination dynamics, a process indicative of MPA or MEG taking place in these systems.[27] TAS experiments were also conducted with ligand-exchanged QD-TBAI solid films (Figure 1c) and a full-stack QDSC (Figure 1d) as a function of light fluence.[28] The results in Figure 1c,d reveal the disappearance of the picosecond Auger process in these systems (at least in the range of exciton fluences studied, 4.1×10^{17}–1.4×10^{19} cm^{-3}) and the appearance of a new and slower relaxation process which we tentatively assign to bimolecular recombination of photogenerated charges. The assignment is based on the low binding energy of excitons in PbS QD[17] and the observation of excitation intensity dependence of the kinetics on the nanosecond timescale which is the typical behavior for thermally activated

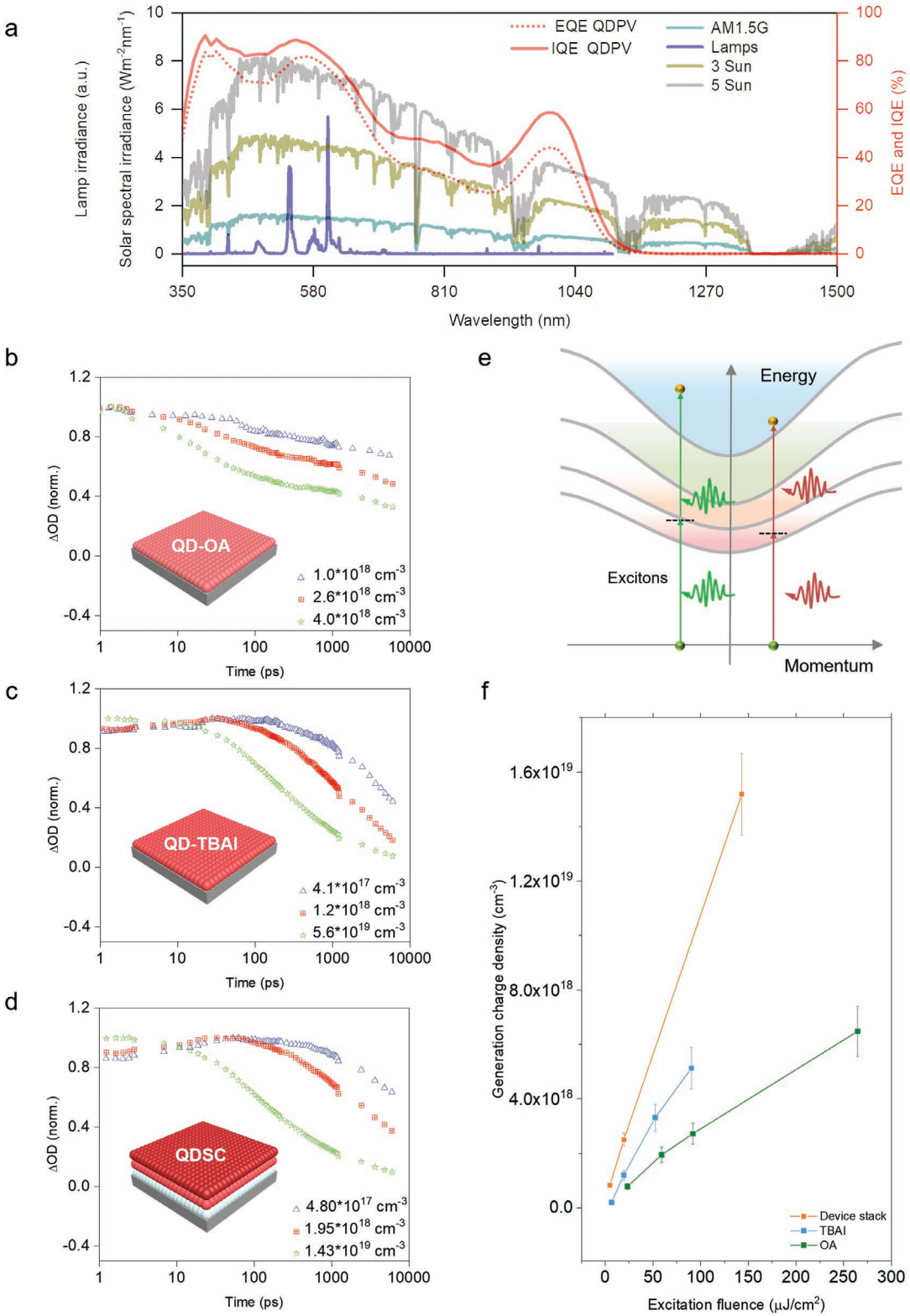

Figure 1. Various light spectra and QD solid film and device MPA ultrafast exciton dynamics. a) The spectra of AM 1.5G and low-concentration (e.g., 3 and 5 Suns) solar irradiance, a fluorescent lamp (1000 lux), and the QE (external and internal) spectra derived from 1.24 eV PbS QDs. Transient absorption kinetics recorded for QD with an oleic acid ligand (b), QD solid thin film with TBAI ligand (c), and full device stack (d), demonstrating the transition from Auger to bimolecular charge recombination losses with ligand exchange. e) Schematic illustrating the MPA process in QD solids. f) Charge densities generated as a function of light fluence, estimated from the lowest energy bleach signal in the transient absorption spectra of the dots and recorded using 526 nm excitation pulse.

charge hopping.[29] The observations of a bleach signal rise seen in Figure 1f,g and shifting of the bleach peak maximum seen in Figure S4, Supporting Information, are consistent with this picture; they also indicate a thermalization process through a density of trap states and the spatial charge hopping between QDs in the QD-TBAI and full-stack QDSC samples.[17,30] A likely cause of the suppression of Auger recombination is closer packing and stronger inter-dot coupling in the TBAI-ligand-exchanged QD allowing fast charge escape into neighbouring QD.[31,32] The suppression of Auger recombination and the slowing down of the charge losses significantly improves the linear response of the active layer to increasing light intensities (Figure 1f), suggesting that devices can principally generate photocurrent linearly above 1 Sun photon flux, provided that charge extraction rates are competitive with the bimolecular recombination losses at J_{sc} and maximum power point (MPP) conditions. It should be noted that the full device stacks exhibited better linear relationship between the excitation fluence and charge generation. We believe the reason could be the energetic gradient created by the multiple layers within the full device stack, where there are layers of QD with different band edge energies,[32] which would enable more effective separation and extraction of charges. It could also be better band bending when packing the QD in the full device stack due to extra material treatment compared to the single QD-TBAI films.[33,9] Therefore, based on these observations, we focus on investigating the response of QDSCs under varying light circumstances from low density indoor to concentrated over 5 Sun irradiation.[21,34]

We start our device performance evaluations under short wavelength light irradiance by first recording the QDSC JV curves at light levels equivalent to indoor fluorescent lamps. **Figure 2**a shows a series of *J–V* curves obtained under different luminance values (i.e., 200 to 2000 lux; Figure S5, Supporting

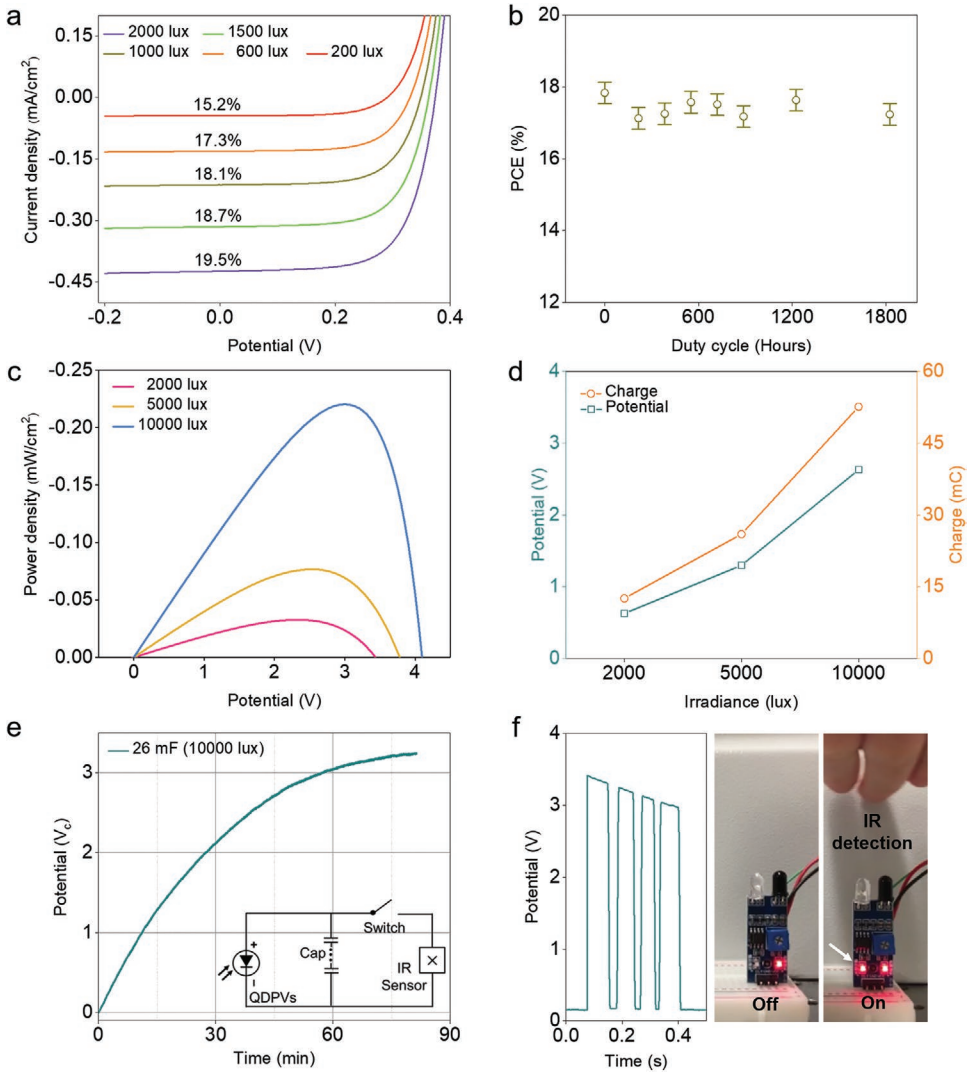

Figure 2. Indoor performance of QDSCs and an integrated IoT sensor module. a) *J–V* curves and PCE values at different room light irradiance levels. b) The unencapsulated QDSC PCE stability performance under 1000 lux insolation for a continuous 1800 h exposure. c,d) Power, photovoltage, and charge from the integrated QDSC circuits as a function of the ambient indoor irradiance. e) Capacitor charging curve under ambient light; inset describes an integrated circuit of QDSCs, capacitors, and an IR sensor. f) Snapshots and transient signals from the IR sensor.

Information) that cover most indoor-light levels.[35,36] An enhancement of J_{sc}, V_{oc}, and the output power density as a function of the input power density can be observed. Consequently, the resulting PCE values from these light sources were up to 19.5%, which are higher than the one Sun world-record performance (≈13%).[10,14] Furthermore, due to the considerable shunt resistance and ideal factor (Figures S6 and S7 and Tables S1 and S2, Supporting Information), a proportional increase in the FF was observed as the light density increased. Moreover, as shown in Figure 2b, the unencapsulated QDSC exhibits outstanding 1800 h stability under the high energy light exposure (Figure S6, Supporting Information), which demonstrates the potential of QDSCs for indoor PV applications such as powering the Internet of Things (IoT) or portable electronic devices.[36,37] To demonstrate the viability of QDSCs for indoor-light-sensor network applications, we integrated an IoT circuit consisting of QDSCs and sensors (Figure S8, Supporting Information). Figure 2c,d shows that the QDSCs produce a 19.21 µW power output (i.e., 52.6 mC) and 2.63 V potential and can readily charge the integrated capacitors. As shown in Figure 2e,f, our IoT module can be successfully powered by the QDSCs matrix to detect the motion of an object, for example, a hand, and activated the alarm. Furthermore, we also dynamically tracked the sensing process, which indicates that indoor QDSC modules can continuously power IR motion sensors.

To assess the response of the QDSC at a higher light irradiance, we used QDSCs under simulated concentrated sunlight conditions. In Figures S9–S11, Supporting Information, the QDSC efficiency notably increased, and the optimized viable input power density range from our concentrated PV (CPV) simulation system is from 1000 to 5001 W m^{-2}. As observed from our TAS analysis, the suppression of Auger recombination significantly improves the linear response of the active layer to increasing light intensities (Figure 1f). Therefore, it can be expected that the QDSCs can principally increase their performance with photon flux provided that charge extraction rates are competitive with the bimolecular recombination loss rates. **Figure 3**a shows the statistics of PCEs for the entire device population under 1–5 Suns concentrations. Indeed, we observe an increase in the PCE with increasing light intensity, which is, however, nonlinear. Notably, the PCE reaches a substantial value of 11.6% (Figure 3a inset) at a 1.5 Sun concentration with ≈30% enhancement from just a normal solid-state ligand exchanged QDSC (with one Sun PCE of ≈9%). It should be noted that though the main limitation remains the fill factor (FF), the simultaneous enhancement of power output and a stable MPP voltage ratio (0.71 ± 0.02) were observed (Figure S12a, Supporting Information), and there is no significant deterioration until intensities above 5 Suns.[35,38]

At these light irradiance levels, we would expect the FF to increase monotonically with increasing charge-carrier density within the QD film and not reduce with increasing light intensity.[4,6] We found QDSC PCE (η) evolution arises due to disproportional changes in the J_{sc}, FF, and V_{oc} with the photon-flux power input (P_{in}) (Figure S12b, Supporting Information, $\eta = \frac{FF \times J_{sc} \times V_{oc}}{P_{in}} \times 100\%$).[6] We note that we did not actively cool the devices during the increasing irradiance tests which may have contributed to the V_{oc} and FF deterioration, since V_{oc} drops with increasing temperature.[4,39] As described in Figure S13 and Table S4, Supporting Information, due to the high cell operation temperature, the parasitic resistance decreases as a function of the solar concentration, which causes the FF to be nonlinear.[40]

One of the potential merit of QDSC is its good ambient tolerance since all the QDSCs are fabricated at ambient condition without any encapsulation.[9,10,33] To access the stability of QDSCs under high irradiance, we measured unencapsulated QDSCs under concentrated sunlight (3 Suns) and list the results in Figure 3b. This light flux was chosen for the stability study because of the high-power output (32.4 ± 0.1 mWcm^{-2}) and high PCE (10.8 ± 0.04%) of the QDSC devices. Encouragingly, we observe good stability under the continuous light exposure at 3 Suns, with the cell maintaining 99% of its original efficiency within 10 h of testing, giving a promise of long-term stability of QDSC for outer space panels and low centration CPVs.[25]

To experimentally demonstrate QDSCs are particularly promising for low-concentration CPV applications, we fabricated a solution-processed QD CPV using a polydimethylsiloxane (PDMS) polymer lens with a solar concentration ratio around 3.[40] The ray trajectory simulations determined that the 2.3 and 4.08 maximum concentration ratios can be achieved through as-prepared 70° and 140° polymer lenses (Figure 3c,d; Figure S14 and Table S5, Supporting Information). The lens-integrated module cell current density (MJ) was revealed by the EQE (Figure 3e) and MJ-V curves (Figure 3f). Assuming that the QDSC and polymer lens are integrated (i.e., P_{in} = 100 mW cm^{-2}), these solution-processed QD CPV systems generate an MPD of 21 mW cm^{-2}, which translates into a considerably high MPCE of 21.29% close to commercialized thin-film PVs.[41] As shown in Figure 3f, a three-fold larger MPCE value can be obtained by covering the QDSC with a 140° polymer lens. These QD CPV systems exhibit stability under high-intensity light irradiation, as summarised in Figure S15, Supporting Information, and Table S6, Supporting Information, presents data from 6 h testing under continuous light exposure. Moreover, we demonstrated conceptual "water lens" QD CPV systems by manipulating the surface tension of the ITO glass side through forming SAM (self-assembled monolayers) layers. Encouragingly, a significant MPCE and power output can be obtained from this water lens system, which further confirmed the potential and moisture environmental stability of integrated QD CPV systems (Figure S16 and Table S7, Supporting Information).

In **Figure 4**a, we summarise the measured J_{SC} and V_{OC} for the unencapsulated devices studied herein under different light intensities. We observe a linear increase in the J_{sc} and a semi-logarithmic increase in the V_{oc} with increasing light intensity (0.01 to 1000 mW cm^{-2}). The performance of the devices is further analyzed and compared with state-of-the-art PbS QDSCs in Figure 4b and Table S8, Supporting Information, where QDSCs are categorized according to the lighting environments used in the experiments, such as sunlight, indoor light, and high-intensity light. Besides the polymer lens integrated QD CPV, the best performance of bared QDSC is under diffused indoor light irradiance, which indicates QDSC may also be suitable for compensating low irradiance in high

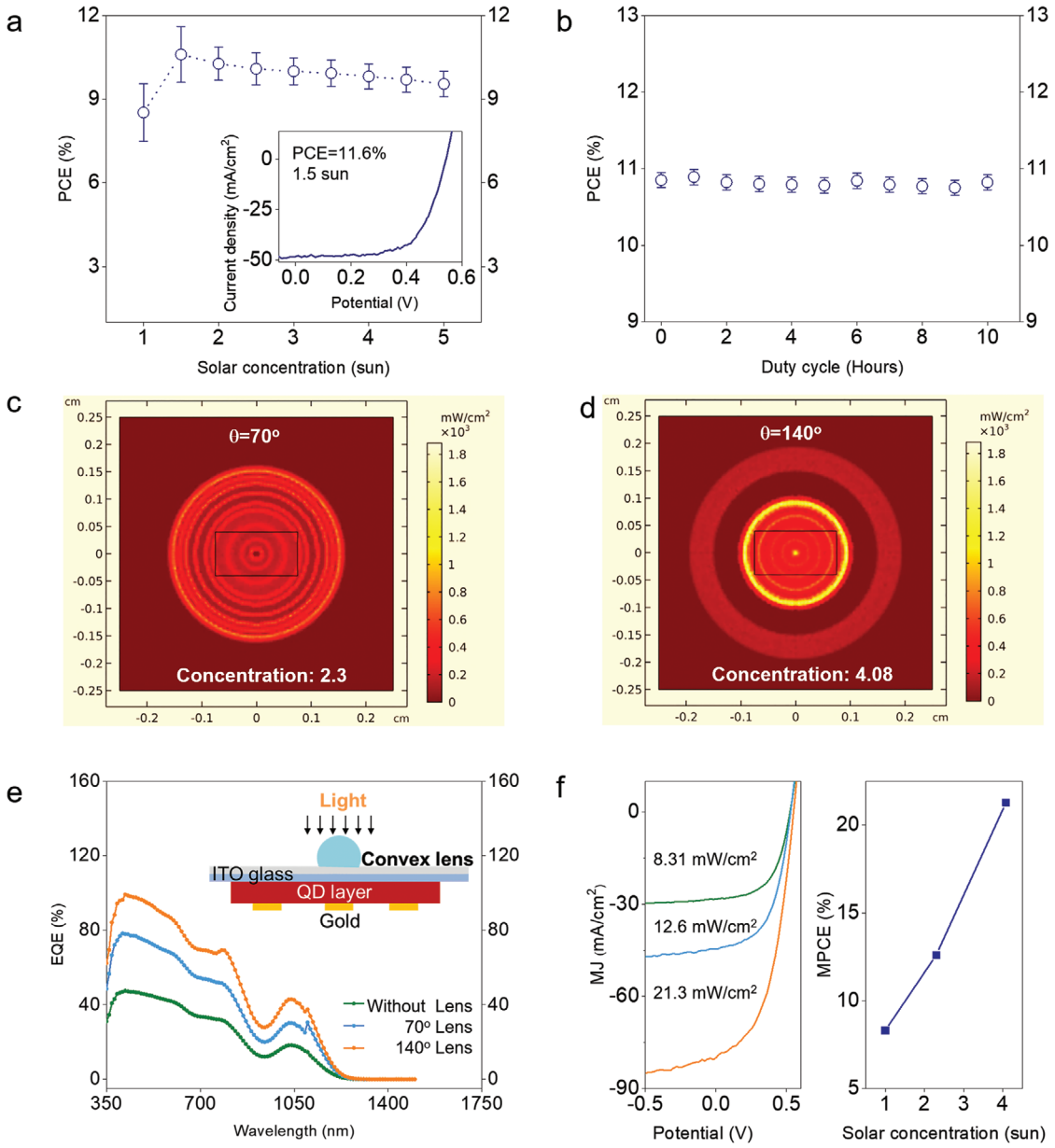

Figure 3. QD CPV system and integrated polymer-lens CPV system characteristics. a) PCE performance of QDSCs under different solar concentrations. The inset displays the *J–V* curve of the as-prepared champion cell. b) Unencapsulated QDSC PCE stability performance under 3 Suns insolation for a continuous 10 h exposure. c,d) Ray trajectories simulated with COMSOL Multiphysics emanating from a 70° and 140° contact angle micro-lens. e) EQE curves of the QD polymer-lens CPV system under 1.5G AM irradiance. Inset of (e) shows the structure of the QD CPV system. f) MJ-V, and MPCE as a function of the solar concentration ratio.

latitude areas (LA). This effect is shown in Figure 4c, where we report the QDSC efficiency under annual daily irradiance conditions from various LA. We give a full description of our estimations in Table S9 and Figure S17, Supporting Information. As highlighted in the periphery of the contour maps (Figure 4c; Figure S18, Supporting Information), a remarkable amount of power can be efficiently generated under various light illumination conditions and adequately attuned for the irradiance difference due to LA variations (e.g., high LA regions or dark intervals).[42]

3. Conclusion

In summary, we have observed excellent performance and good stability of QDSCs under an indoor and concentrated solar irradiance of over four decades for irradiance power densities from 0.01 to 1000 mW cm^{-2}. By investigating the ultrafast exciton dynamics of QDs solids and device stacks, we found that replacement of OA with TBAI ligand suppresses Auger recombination and enhances charge diffusion within the devices. The suppression of Auger recombination and slowing

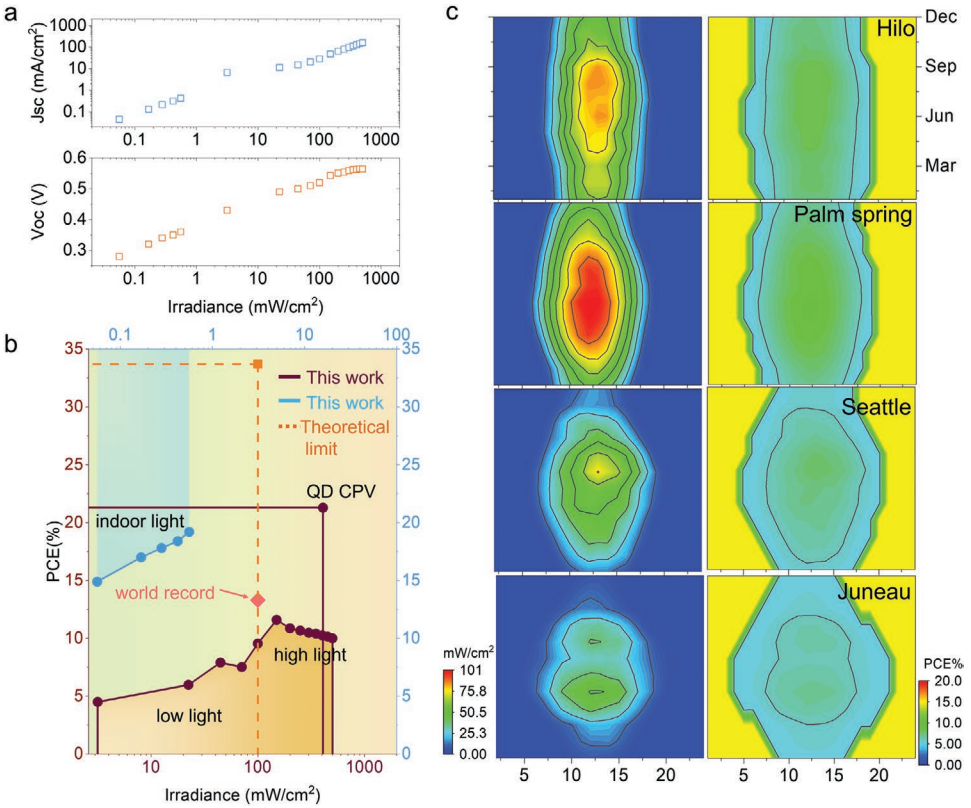

Figure 4. QDSC performance under various lighting conditions. J_{sc} and V_{oc} (a) and PCE (b) evolution under variable ambient (indoor) and solar (sunlight, high-intensity light) irradiance levels. ■ is theoretical limit-based Shockley–Queisser equation and ♦ is the current PbS QDSC world record.[14] The J_{sc}, irradiances are plotted in logarithm scale; V_{oc} and PEC are plotted in linear scale. c) Left panel shows mean annual daily irradiance of four U.S. cities among different LA; right panel shows simulated mean annual daily QDSC efficiency from selected cities.

down of charge losses indicated that the photocurrent of the QDSCs can increase simultaneously with photon flux, provided that the charge extraction rates are competitive with the bimolecular recombination losses at short circuit and maximum power point conditions. Based on these findings, we show a 19.5% (2000 lux indoor light), and an 11.6% efficiency (1.5 Suns) can be easily obtained from a very ordinary solid-state ligand exchanged QDSCs (9.55% under 1 Sun). We further achieve a 21.29% efficiency based on polymer lens CPVs and demonstrate viable indoor sensor networks from QDSCs matrix. In the end, we demonstrated unencapsulated QDSC can generate enough power to remedy insufficient irradiance in high LA regions. We expect that the material innovation and fast developments in the research field of metal chalcogenide PVs will realize non-toxic QDSCs in the near future which could enable QD CPV and indoor cells for green energy supply in our daily life.

4. Experimental Section

Synthesis and Purification of PbS and ZnO QDs: PbS and ZnO QDs were synthesized using previously reported methods.[9,23] All chemicals were purchased from Sigma Aldrich and used without further purification.

Femtosecond Transient Absorption Spectroscopy for QD Solution and Thin Films: The as-prepared QDs were precipitated from toluene by adding an excess of acetone, and the mixture was centrifuged at 8000 rpm for 10 min. After vacuum drying the QDs, they were dispersed in tetrachloroethylene to form a homogeneous, colloidal, stable solution with absolute infrared transparency. The concentration of the PbS QDs was pre-fixed to an optical density (OD) of 0.07 at the first exciton peak. Film QD samples were prepared as follows: glass/QDs with pristine OA ligand; glass/QDs with TBAI ligand; ITO/ZnO/QDs with TBAI ligand/QDs with 1,2-ethanedithiol (EDT) ligand following procedures for device preparation. All films were prepared with 0.25(±0.03) absorbance at their lowest energy excitonic peak maximum.

Fs-TAS analysis was carried out using a HELIOS (Ultrafast Systems) transient absorption spectrometer seeded with 800 nm 100 fs pulses generated at 1 KHz by a Solstice Ti: Sapphire regenerative amplifier (Newport Ltd).[28,43] A TOPAS (Light conversion) optical parametric amplifier was used to generate the excitation pulses, and their intensity was attenuated using a gradual neutral density filter. Experiments were conducted at a standard temperature and pressure conditions. Solution measurements were carried out using a quartz cuvette with a 2-mm beam path with an inserted magnetic stirrer, while films were measured in a 2 cm quartz cuvette put under constant nitrogen pressure. Degradation was not observed during the experiments. Pump pulse energies were measured with Vega Ophir power meter. Film thicknesses for the calculation of exciton densities used in the TAS experiments were measured using KLA Tencor D-600 profilometer.

Device fabrication: A QDSC was fabricated using a modified version of previously reported methods.[9,23] ITO substrates were treated with oxygen plasma for 5 min before the device fabrication. ZnO QDs (50 mg mL^{-1}) were spin-coated onto ITO substrates at 2000 rpm for 30 s. Then, the ZnO QD solid film was annealed at 250 °C over a period of 30 min and then allowed to cool down to room temperature. The PbS QD solid film was fabricated via a layer-by-layer spin-casting protocol:

i) A PbS QD solution (50 mg mL^{-1}) was spin cast onto the substrate at 2000 rpm for 15 s. ii) A tetrabutylammonium iodide (TBAI) solution (10 mg mL^{-1} in methanol) was drop cast onto the substrate for 30 s and spun at 2000 rpm for 30 s to form a QD film. This film was then rinsed twice with methanol before applying a subsequent QD layer (ten layers in total). iii) An EDT solution (0.02% volume in acetonitrile) was applied to the substrate via spin casting after the deposition of the PbS QD solution. After washing twice with acetonitrile, the final device was transferred into a thermal evaporator. Au contact pins were thermally evaporated onto the films through shadow masks. The device areas were defined by applying 0.012 cm^2 masks.

Integrated QDSC and Sensor Circuit Fabrication: The demonstration circuit for the sensor application consists of QDSCs (ten cells were connected in series), capacitors (10–30 mF), a switch, and an IR motion sensor. Commercially available IR motion sensor, capacitors, and 2000 lux fluorescent light (Phillips) were used for the demonstration. Equivalent circuit and detail circuit parameters can be found in Figure 2e and Figure S8 and Table S3, Supporting Information.

Device Characterization: Solar cell measurement protocols are provided in Figure S19 and Table S10, Supporting Information. These protocols were used for evaluating QDSC performance and stability under sunlight, indoor-light, and high-intensity light irradiance. The AM 1.5G *J–V* curves were recorded using a Keithley 2400 instrument under simulated solar light illumination from a LOT Quantum Design simulator (LSE340/1/850.27C) equipped with 300 W Xe arc lamps. The light intensity was calibrated using a RERA SOLUTIONS silicon reference cell (RQS4695) before each measurement. The ambient low-light (200 to 10000 lux) *J–V* curves were obtained using a Keithley 2400 source meter under a series of fluorescent lamps with reflectors (Osram L18W/827). The lux levels of the fluorescence lamps were measured by a lux meter (LX-1330B). The light intensity of the fluorescent lamps was calibrated by a Thorlabs PM100D power and energy meter equipped with a Thorlabs S401C high-sensitivity thermal sensor. A series of OD filters was employed to obtain different light intensities under 1 Sun illumination. The high-intensity light (1 Sun to 30 Suns) *J–V* curves were obtained using a Class AAA solar simulator system (WXS-220S-L2, Wacom, KANC, as shown in Figure S7, Supporting Information) equipped with a xenon lamp (×1), halogen lamps (×3), Fresnel lens, and IR/UV filters to achieve different sun irradiance levels. The effective irradiated area was from 484 cm^2 (1 Sun) to 0.25 cm^2 (500 Suns).

Quantum Efficiency (EQE and IQE): A SpeQuest quantum efficiency (QE) system was employed to measure the external quantum efficiency (EQE) and internal quantum efficiency (IQE). The QE system had a 100 W quartz tungsten halogen light and 150 mm F/4.2 monochromator as a photon source and an SR830 DSP lock-in amplifier (locked to light chopped at 83 Hz) and a Melles Griot IV converter to extract the photocurrent. The wavelength range was from 350 to 1800 nm, and all the measurements were calibrated using NIST silicon (200-1100 nm) and germanium (700-1800 nm) reference cells with areas pre-defined by a mask (0.012 cm^2). To measure the IQE, the EQE was measured, and then, the reflected signal (light) was excluded. An integrated sphere (Ocean Optics ISP-30-6-R) was employed to measure the reflected signal (direct and diffuse reflections), and a reflectance standard was applied to calibrate the system before each measurement.

Polymer Microlens Fabrication: A PDMS elastomer base (Sylgard 184, Dow Corning) was mixed with the curing agent at a weight ratio of 20:1 and degassed at room temperature for 1 h. Then, 0.02–0.04 mL of the PDMS solution was dropped onto a preheated hot plate with a syringe and allowed to solidify in the temperature range of 200–300 °C for 1 min. The geometrical properties of the PDMS lens were controlled by the heating temperature for a fixed droplet volume and height. For instance, the angles of 70° and 140° with a diameter of 0.5–0.7 cm (minimum 0.5 cm) were fabricated at 200 and 280 °C, respectively.

Ray Trajectory Simulation: Polymer lens concentrator simulations were performed using the Ray Optics module of the COMSOL Multiphysics software suite. As shown in Figure S15, Supporting Information, the geometric profiles were interpolated from the two fabricated microlenses with contact angles of $\theta_1 = 140°$ and $\theta_2 = 70°$. In each case, a 100 mW cm^{-2} initial flux density (I_{in}) was applied to the lens surface using an illuminated surface boundary condition, and only the refracted rays were evaluated. The number of calculated beams was $N = 10^5$. A rectangular surface, that is, a focal plane, was placed 1.1 mm away from the lens to match the thickness of the ITO glass. By applying a wall boundary condition, the incident flux density (I_f) on the active area of the focal plane was calculated as $A = 0.08 \times 0.15$ cm^2. The local concentration ratio (R) was evaluated using the equation

$$R = \frac{I_f}{I_{in}} \tag{1}$$

Detailed simulation parameters are listed in Table S5, Supporting Information.

Supporting Information

Supporting Information is available from the Wiley Online Library or from the author.

Acknowledgements

The authors acknowledge funds from the National Research Foundation (NRF) of Korea (2019R1A2C1005930), the Engineering and Physical Sciences Research Council (EPSRC, EP/P027628/1), and the European Commission Horizon 2020 (685758). Also, the authors would like to thank the Sêr Solar initiative and the European regional development fund through the Welsh government. S.D. would like to thank Amirah Way for support with experiments. B.H. would like to acknowledge the financial support by the Cardiff University as well as EPSRC (EP/K040375/1) for funding the "South of England Analytical Electron Microscope" used in this research.

Conflict of Interest

The authors declare no conflict of interest.

Author Contributions

B.H. and B.-S.K. contributed equally to this work. B.H. and S.C. conceived the experiments and led the project. B.H. and B.S.K. performed material synthesis, device fabrication, and characterization. K.H.L., W.C.T., and Z.L. performed the indoor PV characterization and analysis. S.D. and M.D. conducted the fs-TAS analysis. Y.C. and P.G. performed the circuit construction and ray trajectories simulation. J.D. and J.K. contributed to scientific discussion and provided experimental guidance. M.X.L., J.Z., S.D., and J.S. contributed to the interpretation of the data and commented on the manuscript. B.H. S.D. and S.C. wrote the paper with input and discussion from all authors.

Keywords

concentration photovoltaics, indoor solar cells, multi-photon absorption, PbS quantum dots, ultrafast transient absorption spectroscopy

Received: May 28, 2020
Published online: August 11, 2020

[1] S. Chu, Y. Cui, N. Liu, *Nat. Mater.* **2017**, *16*, 16.
[2] a) M. Freitag, J. Teuscher, Y. Saygili, X. Zhang, F. Giordano, P. Liska, J. Hua, S. M. Zakeeruddin, J.-E. Moser, M. Grätzel, A. Hagfeldt, *Nat.*

Photonics **2017**, *11*, 372; b) D. M. Chapin, C. S. Fuller, G. L. Pearson, *J. Appl. Phys.* **1954**, *25*, 676.
[3] A. Polman, M. Knight, E. C. Garnett, B. Ehrler, W. C. Sinke, *Science* **2016**, 352.
[4] Z. Wang, Q. Lin, B. Wenger, M. G. Christoforo, Y.-H. Lin, M. T. Klug, M. B. Johnston, L. M. Herz, H. J. Snaith, *Nat. Energy* **2018**, *3*, 855.
[5] F. Meinardi, S. Ehrenberg, L. Dhamo, F. Carulli, M. Mauri, F. Bruni, R. Simonutti, U. Kortshagen, S. Brovelli, *Nat. Photonics* **2017**, *11*, 177.
[6] J. Nelson, *The Physics of Solar Cells*, Imperial College Press, London **2003**.
[7] a) T.-H. Kim, D.-Y. Chung, J. Ku, I. Song, S. Sul, D.-H. Kim, K.-S. Cho, B. L. Choi, J. Min Kim, S. Hwang, K. Kim, *Nat. Commun.* **2013**, *4*, 2637; b) T.-H. Kim, K.-S. Cho, E. K. Lee, S. J. Lee, J. Chae, J. W. Kim, D. H. Kim, J.-Y. Kwon, G. Amaratunga, S. Y. Lee, B. L. Choi, Y. Kuk, J. M. Kim, K. Kim, *Nat. Photonics* **2011**, *5*, 176; c) K.-S. Cho, E. K. Lee, W.-J. Joo, E. Jang, T.-H. Kim, S. J. Lee, S.-J. Kwon, J. Y. Han, B.-K. Kim, B. L. Choi, J. M. Kim, *Nat. Photonics* **2009**, *3*, 341.
[8] V. Adinolfi, E. H. Sargent, *Nature* **2017**, *542*, 324.
[9] B. Hou, Y. Cho, B. S. Kim, J. Hong, J. B. Park, S. J. Ahn, J. I. Sohn, S. Cha, J. M. Kim, *ACS Energy Lett.* **2016**, *1*, 834.
[10] M. Liu, O. Voznyy, R. Sabatini, F. P. Garcia de Arquer, R. Munir, A. H. Balawi, X. Lan, F. Fan, G. Walters, A. R. Kirmani, S. Hoogland, F. Laquai, A. Amassian, E. H. Sargent, *Nat. Mater.* **2017**, *16*, 258.
[11] B. Sun, O. Ouellette, F. P. García de Arquer, O. Voznyy, Y. Kim, M. Wei, A. H. Proppe, M. I. Saidaminov, J. Xu, M. Liu, P. Li, J. Z. Fan, J. W. Jo, H. Tan, F. Tan, S. Hoogland, Z. H. Lu, S. O. Kelley, E. H. Sargent, *Nat. Commun.* **2018**, *9*, 4003.
[12] M. J. Speirs, D. N. Dirin, M. Abdu-Aguye, D. M. Balazs, M. V. Kovalenko, M. A. Loi, *Energy Environ. Sci.* **2016**, *9*, 2916.
[13] J. Xu, O. Voznyy, M. Liu, A. R. Kirmani, G. Walters, R. Munir, M. Abdelsamie, A. H. Proppe, A. Sarkar, F. P. García de Arquer, M. Wei, B. Sun, M. Liu, O. Ouellette, R. Quintero-Bermudez, J. Li, J. Fan, L. Quan, P. Todorovic, H. Tan, S. Hoogland, S. O. Kelley, M. Stefik, A. Amassian, E. H. Sargent, *Nat. Nanotechnol.* **2018**, *13*, 456.
[14] M.-J. Choi, F. P. García de Arquer, A. H. Proppe, A. Seifitokaldani, J. Choi, J. Kim, S.-W. Baek, M. Liu, B. Sun, M. Biondi, B. Scheffel, G. Walters, D.-H. Nam, J. W. Jo, O. Ouellette, O. Voznyy, S. Hoogland, S. O. Kelley, Y. S. Jung, E. H. Sargent, *Nat. Commun.* **2020**, *11*, 103.
[15] S.-W. Baek, S. Jun, B. Kim, A. H. Proppe, O. Ouellette, O. Voznyy, C. Kim, J. Kim, G. Walters, J. H. Song, S. Jeong, H. R. Byun, M. S. Jeong, S. Hoogland, F. P. García de Arquer, S. O. Kelley, J.-Y. Lee, E. H. Sargent, *Nat. Energy* **2019**, *4*, 969.
[16] a) A. J. Nozik, *Phys. E* **2002**, *14*, 115; b) P. V. Kamat, *J. Phys. Chem. Lett.* **2013**, *4*, 908; c) B. Hou, *Isr. J. Chem.* **2019**, *59*, 637.
[17] A. H. Proppe, J. Xu, R. P. Sabatini, J. Z. Fan, B. Sun, S. Hoogland, S. O. Kelley, O. Voznyy, E. H. Sargent, *Nano Lett.* **2018**, *18*, 7052.
[18] G. H. Carey, A. L. Abdelhady, Z. Ning, S. M. Thon, O. M. Bakr, E. H. Sargent, *Chem. Rev.* **2015**, *115*, 12732.
[19] M. T. Trinh, A. J. Houtepen, J. M. Schins, T. Hanrath, J. Piris, W. Knulst, A. P. L. M. Goossens, L. D. A. Siebbeles, *Nano Lett.* **2008**, *8*, 1713.
[20] a) M. C. Beard, J. C. Johnson, J. M. Luther, A. J. Nozik, *Philos. Trans. R. Soc., A* **2015**, *373*, 20140412; b) N. S. Makarov, P. C. Lau, C. Olson, K. A. Velizhanin, K. M. Solntsev, K. Kieu, S. Kilina, S. Tretiak, R. A. Norwood, N. Peyghambarian, J. W. Perry, *ACS Nano* **2014**, *8*, 12572; c) C. M. Cirloganu, L. A. Padilha, Q. Lin, N. S. Makarov, K. A. Velizhanin, H. Luo, I. Robel, J. M. Pietryga, V. I. Klimov, *Nat. Commun.* **2014**, *5*, 4148; d) G. Nair, L.-Y. Chang, S. M. Geyer, M. G. Bawendi, *Nano Lett.* **2011**, *11*, 2145; e) R. D. Schaller, V. I. Klimov, *Phys. Rev. Lett.* **2004**, *92*, 186601; f) R. G. Ispasoiu, Y. Jin, J. Lee, F. Papadimitrakopoulos, T. Goodson, *Nano Lett.* **2002**, *2*, 127.
[21] L. A. Padilha, G. Nootz, P. D. Olszak, S. Webster, D. J. Hagan, E. W. Van Stryland, L. Levina, V. Sukhovatkin, L. Brzozowski, E. H. Sargent, *Nano Lett.* **2011**, *11*, 1227.
[22] Y. Yan, R. W. Crisp, J. Gu, B. D. Chernomordik, G. F. Pach, A. R. Marshall, J. A. Turner, M. C. Beard, *Nat. Energy* **2017**, *2*, 17052
[23] B. Hou, Y. Cho, B.-S. Kim, D. Ahn, S. Lee, J. B. Park, Y.-W. Lee, J. Hong, H. Im, S. M. Morris, J. I. Sohn, S. Cha, J. M. Kim, *J. Mater. Chem. C* **2017**, *5*, 3692.
[24] Y. Wang, Z. Liu, N. Huo, F. Li, M. Gu, X. Ling, Y. Zhang, K. Lu, L. Han, H. Fang, A. G. Shulga, Y. Xue, S. Zhou, F. Yang, X. Tang, J. Zheng, M. Antonietta Loi, G. Konstantatos, W. Ma, *Nat. Commun.* **2019**, *10*, 5136.
[25] M. A. Green, S. P. Bremner, *Nat. Mater.* **2017**, *16*, 23.
[26] a) M. C. Beard, J. M. Luther, O. E. Semonin, A. J. Nozik, *Acc. Chem. Res.* **2013**, *46*, 1252; b) I. Kang, F. W. Wise, *J. Opt. Soc. Am. B* **1997**, *14*, 1632.
[27] R. J. Ellingson, M. C. Beard, J. C. Johnson, P. Yu, O. I. Micic, A. J. Nozik, A. Shabaev, A. L. Efros, *Nano Lett.* **2005**, *5*, 865.
[28] a) S. D. Dimitrov, M. Azzouzi, J. Wu, J. Yao, Y. Dong, P. S. Tuladhar, B. C. Schroeder, E. R. Bittner, I. McCulloch, J. Nelson, J. R. Durrant, *J. Am. Chem. Soc.* **2019**, *141*, 4634; b) S. D. Dimitrov, S. Wheeler, D. Niedzialek, B. C. Schroeder, H. Utzat, J. M. Frost, J. Yao, A. Gillett, P. S. Tuladhar, I. McCulloch, J. Nelson, J. R. Durrant, *Nat. Commun.* **2015**, *6*, 6501.
[29] J. Nelson, *Phys. Rev. B* **2003**, *67*, 155209.
[30] R. H. Gilmore, E. M. Y. Lee, M. C. Weidman, A. P. Willard, W. A. Tisdale, *Nano Lett.* **2017**, *17*, 893.
[31] a) B.-S. Kim, J. Hong, B. Hou, Y. Cho, J. I. Sohn, S. Cha, J. M. Kim, *Appl. Phys. Lett.* **2016**, *109*, 063901; b) D. Bederak, D. M. Balazs, N. V. Sukharevska, A. G. Shulga, M. Abdu-Aguye, D. N. Dirin, M. V. Kovalenko, M. A. Loi, *ACS Appl. Nano Mater.* **2018**, *1*, 6882.
[32] B. Kundu, A. J. Pal, *J. Phys. Chem. C* **2018**, *122*, 11570.
[33] C.-H. M. Chuang, P. R. Brown, V. Bulović, M. G. Bawendi, *Nat. Mater.* **2014**, *13*, 796.
[34] M. E. Schmidt, S. A. Blanton, M. A. Hines, P. Guyot-Sionnest, *Phys. Rev. B* **1996**, *53*, 12629.
[35] H. K. H. Lee, Z. Li, J. R. Durrant, W. C. Tsoi, *Appl. Phys. Lett.* **2016**, *108*, 253301.
[36] A. Nasiri, S. A. Zabalawi, G. Mandic, *IEEE Trans. Ind. Electron.* **2009**, *56*, 4502.
[37] J. W. Matiko, N. J. Grabham, S. P. Beeby, M. J. Tudor, *Meas. Sci. Technol.* **2014**, *25*, 012002.
[38] M. A. Husain, A. Tariq, S. Hameed, M. S. B. Arif, A. Jain, *Green Energy Environ.* **2017**, *2*, 5.
[39] M. T. Hörantner, H. J. Snaith, *Energy Environ. Sci.* **2017**, *10*, 1983.
[40] S. Ekgasit, N. Kaewmanee, P. Jangtawee, C. Thammacharoen, M. Donphoongpri, *ACS Appl. Mater. Interfaces* **2016**, *8*, 20474.
[41] M. A. Green, Y. Hishikawa, W. Warta, E. D. Dunlop, D. H. Levi, J. Hohl-Ebinger, A. W. H. Ho-Baillie, *Prog. Photovoltaics.* **2017**, *25*, 668.
[42] A. Sacco, M. Gerosa, S. Bianco, L. Mercatelli, R. Fontana, L. Pezzati, M. Quaglio, C. F. Pirri, A. O. M. Tucci, *Sol. Energy* **2016**, *125*, 307.
[43] S. D. Dimitrov, Z. Huang, F. Deledalle, C. B. Nielsen, B. C. Schroeder, R. S. Ashraf, S. Shoaee, I. McCulloch, J. R. Durrant, *Energy Environ. Sci.* **2014**, *7*, 1037.